processes

MDPI

Article

Optimization of the Oxidative Coupling of Methane Process for Ethylene Production

Raed Alkathiri, Ali Alshamrani, Irfan Wazeer, Mourad Boumaza and Mohamed K. Hadj-Kali *

Chemical Engineering Department, King Saud University, P.O. Box 800, Riyadh 11421, Saudi Arabia; raedalkathiri@gmail.com (R.A.); alshamrani.ali20@gmail.com (A.A.); iwazeer@ksu.edu.sa (I.W.); mouradb@ksu.edu.sa (M.B.)

* Correspondence: mhadjkali@ksu.edu.sa

Abstract: The oxidative coupling of methane (OCM) process is considered an intriguing route for the production of ethylene, one of the most demanded petrochemical products on the market. Ethylene can be produced by various methods, but the most widely used is the steam cracking process. However, due to the current instability of the crude oil market and the shale gas revolution, the production of olefins from natural gas has opened a new path for companies to mitigate the high demand for crude oil while utilizing an abundant amount of natural gas. In this work, the OCM process was compared with other existing processes, and the process was simulated using Aspen HYSYS. The flowsheet was divided into four sections, namely (i) the reaction section, (ii) the water removal section, (iii) the carbon dioxide capture section, and (iv) the ethylene purification section. Each section was thoroughly discussed, and the heat integration of the process was performed to ensure maximum energy utilization. The heat exchanger network was constructed, and the results show that the heating utility can be reduced by more than 95% (from 76567 kW to 2107.5 kW) and the cooling utility can be reduced by more than 60% (from 116398 kW to 41939.2 kW) at an optimum minimum temperature difference of 25 °C. In addition, a case study on the recovery of the high exothermic heat of reaction for power production shows that 16.68 MW can be produced through the cycle, which can cover the total cost of compression.

Keywords: natural gas; ethylene; OCM process; process simulation; heat integration

Citation: Alkathiri, R.; Alshamrani, A.; Wazeer, I.; Boumaza, M.; Hadj-Kali, M.K. Optimization of the Oxidative Coupling of Methane Process for Ethylene Production. *Processes* **2022**, *10*, 1085. https://doi.org/10.3390/pr10061085

Received: 3 May 2022
Accepted: 24 May 2022
Published: 29 May 2022

1. Introduction

Ethylene is used throughout the world as an intermediate in the production of plastics and other liquid hydrocarbons such as alpha-olefins [1,2]. These carbon-rich olefins can then be converted to paraffins, resulting in energy-rich liquid fuels [3,4]. Ethylene accounts for a large share of petrochemical production. The global ethylene market was estimated at USD 101.1 billion in 2020 and is expected to grow at a 5.5% compound annual growth rate by 2029 [5]. The last decade has witnessed huge consumption of ethylene. This consumption has been led by the high demand for ethylene derivatives, which are easy to process, lightweight, inexpensive, and of high quality. The consumption of ethylene by application is depicted in Figure S1 in the Supplementary Materials.

In recent years, the price of oil has increased more than the price of natural gas, and forecasts indicate that this trend will continue in the coming years [6]. The "fuel switch" scenario is the result of these forecasts, which drive research efforts towards diversification of feedstocks used for the synthesis of olefins [7,8]. Natural gas is one of the key possibilities for replacing oil at least partially in the production of hydrocarbons, as natural gas deposits are considered more abundant than oil resources. Since it is used as a feedstock to produce many plastics, ethylene is the most widely produced light hydrocarbon in the world, with an annual production of 140–160 million tons [9]. Huge shale gas deposits and the emergence of biogas sources have facilitated access to natural gas, which has increased interest in using methane as a feedstock for the production of

chemicals [10,11]. Furthermore, according to the U.S. Energy Information Administration, coal generates about 200 pounds of CO_2/MMBtu, while crude oil generates 160 pounds of CO_2/MMBtu, a 20% reduction. Methane, on the other hand, produces only 117 pounds of CO_2/MMBtu, which is 41.5% less than coal and 27% less than crude oil [12].

The conventional methods for producing ethylene are the steam and thermal cracking processes. These processes account for most of the world's ethylene production [13]. However, the energy intensity (up to 40 GJ of heat per ton of ethylene) and the lack of sustainability for the environment are two important problems addressed here [13–15]. These methods require high temperatures (>1200 °C) to break the C-H bond (bond energy, 440 kJ/mol), and about three tons of CO_2 are emitted per ton of ethylene produced [11]. Therefore, indirect routes, such as catalytic Fischer–Tropsch synthesis of syngas (CO/H_2), are another way to produce ethylene from natural gas [16,17]. This whole process requires a considerable amount of energy, since in the first phase of this pathway, all four strong C-H bonds in CH_4 are broken without producing free radicals CH_2 or CH_3, which are needed for the direct synthesis of C_{2+} species [6].

For these reasons, efforts have been made in the last three decades to develop a simpler, less expensive, and more sustainable alternative for ethylene production [18]. One of these technologies is the production of ethylene by oxidative coupling of methane (OCM). Direct conversion of CH_4 to ethane and ethylene has the potential to be less harmful to the environment and more economically viable [19]. The OCM process consists of the catalytic oxidation of methane, which has been studied since the 1980s [20] as a promising way to utilize natural gas and, more recently, shale gas as a feedstock for chemical building blocks such as ethylene.

As for the OCM catalyst, several options have been discussed by various researchers. Ito and Lunsford [21], Hinsen and Baerns [22], Keller and Bhasin [20], and Driscoll et al. [23] were the first to attempt to convert methane directly to ethylene and other hydrocarbons. These early studies showed that methane could be effectively converted to ethylene and other hydrocarbons such as ethane and benzene using metal oxide catalysts, albeit at a modest conversion rate and occasionally with low yields. For example, Hinsen and Baerns [22] reported a 5% methane conversion with a 58% ethylene selectivity using a PbO/Al_2O_3 catalyst, while Ito and Lunsford [21] reported a 28% methane conversion with a 50% ethylene selectivity. As a result, most research conducted after these studies focused on the effects of catalyst compositions, modifications, and reaction conditions to achieve high conversion and selectivity. Doping of CaO with alkali metals has been shown to increase catalytic activity towards C_2 compounds (including Li-CaO, Na-CaO, K-CaO, Rb-CaO, Cs-CaO) compared to single oxides [24]. Among CaO doped with alkali metals, Li-CaO, Na-CaO, and K-CaO exhibited better catalytic performance [25]. However, due to the volatility of Li, its stability was found to be limited [24].

A few authors [26,27] have developed two types of metal oxide catalysts, Li-doped TbO_x and Sm_2O_3 on MgO support. The Li-Tb_2O_3/n-MgO catalyst showed high activity and selectivity for the desired products at a low reaction temperature. In addition, the catalyst exhibited greater stability and a lower deactivation rate after 30 h of operation because the addition of Li induced the reduction of TbO_x to Tb_2O_3 and shifted the electrons of the Tb 3d core level to a higher binding energy, resulting in strong Li-TbO_x interactions that made the catalyst more active for the formation of C_2 products than SmO_x. Due to its high selectivity, temperature, and reaction stability, the Mn-Na_2WO_4/SiO_2 catalyst is also considered a good choice for the OCM process. Mn-Na_2WO_4/SiO_2 has been shown to be stable over long periods of time, resulting in methane conversion of 20–30% and combined ethane and ethylene yields of 70–80% [28–30]. Table 1 reports the different available choices of catalysts for the OCM process.

Table 1. Various catalysts used for the OCM process.

Catalyst	Operating Conditions	CH_4 Conversion	Selectivity	Ref.
Na-CaO	T = 750 °C, CH_4/O_2 = 4	24.7	68.8	[25]
K-CaO	WHSV = 5140 $cm^3g^{-1}h^{-1}$	25.2	58.9	
$Mn/Na_2WO_4/SiO_2$	T = 775 °C, CH_4/air = 7.5	20	80	[29]
Li-TbO_x/n-MgO	T = 700 °C, CH_4/O_2 = 4	24.9	63.6	[27]
Li-Sm_2O_3/n-MgO	GHSV = 2400 h^{-1}	24.4	62.5	
Ce-Mn-Na_2WO_4/SiO_2	T = 800 °C, CH_4/air = 1	21	84	[31]
Mn-Na_2WO_4/SiO_2	T = 800 °C, CH_4/air = 2	45.4	41.4	[30]
Mn-Na_2WO_4/n-SiO_2	T = 800 °C, CH_4/O_2 = 4	25.2	73.3	[32]
MnxOy-Na_2WO_4/SiO_2-rutile	T = 750 °C, CH_4/O_2 = 4	6.5	58.6	[33]

The OMC process is still more attractive to the industry. Various reaction pathways have been proposed, but it is generally accepted that the desired selective oxidation pathway results in methane adsorbing on the catalyst surface and being converted to the intermediate ethane [34]. The ethane reacts further, either on the catalyst surface or in the gas phase, to form the main product, ethylene. Since the discovery of OCM in 1982, it has been extensively studied, and several reviews have been published [35–38].

In recent decades, several studies have shown that the OCM process is a promising alternative to steam cracking, but it has not gained acceptance in the industrial market for several reasons. First, OCM has a relatively low ethylene concentration in the product stream compared to the amount of reactant fed. It is difficult to use OCM widely without detailed chemical data on the C_2 yields of the most promising catalysts, which are not widely available. Second, because the OCM reaction is only effective at very high temperatures with hydrocarbons that require very low temperatures for separation, heat integration and efficient operation are critical to a profitable process. According to Vandewalle et al. [39], it appears to be a lack of accurate and up-to-date information on the overall performance of OCM, which is essential for evaluating the process as a viable alternative for industrial-scale C_2H_4 production. Despite decades of efforts to maximize C_2 production in a single OCM reactor, the reactor parameters that would help OCM drive down ethylene prices have yet to be determined. A comprehensive characterization of this process, as well as the selection of the best reactor conditions, would help situate the current state of the art in the context of global ethylene production.

This research focused on the application of the OCM process in a commercial-scale plant, which has the potential for significant gains due to the low cost of natural gas and rising oil prices impacting traditional ethylene production methods. Our main objective was to develop and optimize the process flow diagram by considering each area of the process individually and mentioning the main techniques that can be applied, in addition to improving the heat utilization in the process. To achieve this objective, a pinch analysis was conducted to maximize the heat utilization in the process by determining the minimum heating and cooling utilities that are required as well as identifying the possible heat exchanger network.

2. Comparison between Various Processes to Produce Ethylene

Ethylene is produced in the petrochemical industry in several ways. It is produced primarily by steam cracking of hydrocarbons, converting large hydrocarbons into smaller chains. Ethylene can also be produced by dehydration of ethanol or by oxidative coupling of methane OCM, which is a chemical reaction discovered in the 1980s for the direct conversion of methane into value-added chemicals. These three technologies are presented hereafter.

2.1. Steam Cracking

Currently, the most important technical process for the production of ethylene is the hydrocarbon cracking process. Nearly 99% of the global ethylene is synthesized

by this method because it offers high conversion and selectivity to ethylene [40], but more byproducts can be produced in this process. Hydrocarbon cracking uses petro-hydrocarbon or natural gas, such as naphtha, liquefied petroleum gas, ethane, or propane, as feedstock. Hydrocarbon compounds with a large number of carbon atoms can be cracked into smaller hydrocarbon compounds such as ethylene and propylene at high temperatures [41]. Figure 1 depicts the block flow diagram (BFD) of ethylene production by steam cracking. The main disadvantages of this process are the dependence on fossil fuels for feedstock supply, the huge energy required, and other pollution concerns.

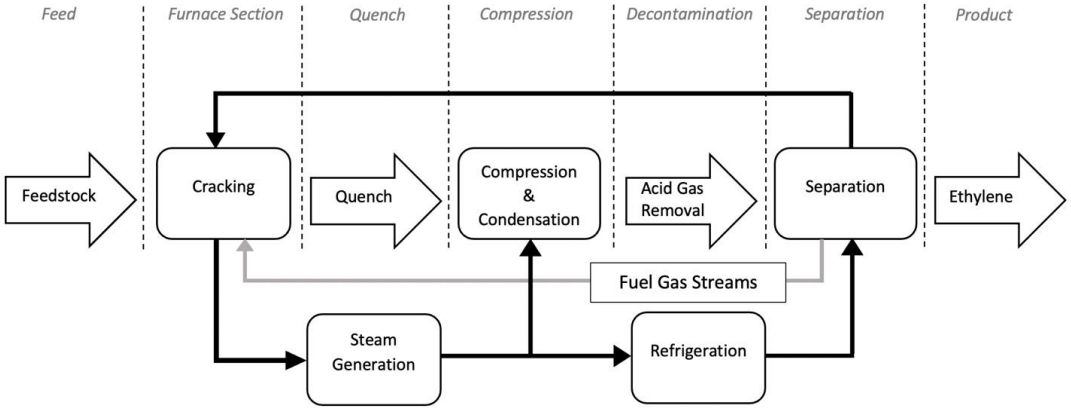

Figure 1. Block flow diagram of ethylene process by steam cracking [42].

2.2. Dehydration of Ethanol

Catalytic dehydration of ethanol to ethylene was the earliest used process in the industry [43]. Considering the establishment of the industrial production facilities [44], the process of dehydrating ethanol to ethylene typically consists of two parts: the ethanol dehydration reaction and the purification of ethylene products, as depicted in Figure 2 [45]. This process is based on three reactions [46]:

$$C_2H_5OH \leftrightharpoons C_2H_4 + H_2O \quad (1)$$

$$C_2H_5OH \rightarrow CH_3CHO + H_2 \quad (2)$$

$$2C_2H_5OH \rightarrow (C_2H_5)_2O + H_2O \quad (3)$$

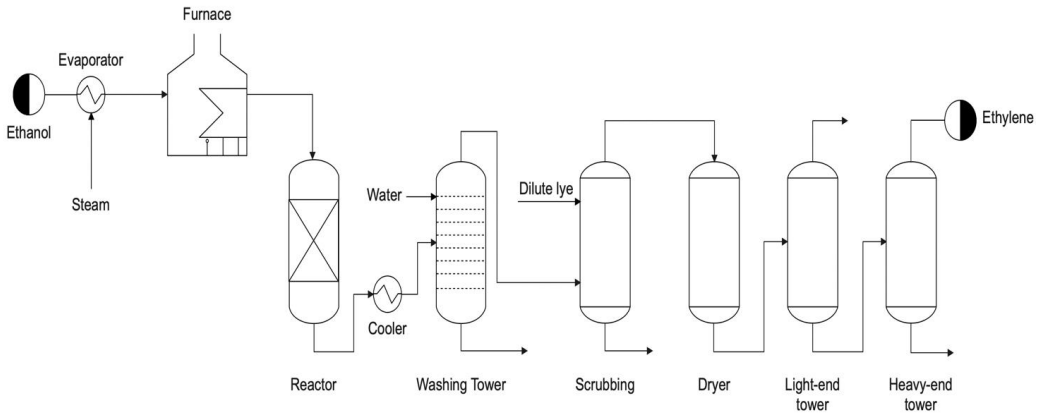

Figure 2. Process flow diagram of ethylene process by dehydration of ethanol [45].

In addition, this process provides high conversion and selectivity to ethylene, making it competitive with the steam cracking process. Nevertheless, with the situation of fossil resources becoming increasingly sparse, the use of biomass ethanol catalytic dehydration to

ethylene has greater development potential and broader application prospects. However, the operating costs are much higher.

2.3. Oxidative Coupling of Methane "OCM"

The OCM is another intriguing route to produce ethylene. It was discovered by Keller and Bhasin in 1982 [20] and has gained attracted much attention from researchers wanting to develop it further and gain a deeper understanding of its nature to make the OCM process highly viable for commercialization. Although OCM can be an attractive method in the ethylene market due to its low cost and wide availability of feedstock, its low selectivity to ethylene due to the high exothermicity [47] has limited its application. Furthermore, a large number of research papers have been published since 1982 detailing how to maximize ethylene yield. Most of the published research focused on the improvement of the catalyst, reactor design, downstream purification techniques, environmental assessment, and economic evaluation [24]. In comparison with the other mentioned processes, OCM is distinguished by the low price of feedstock and its abundance, as countries have a great interest in converting their natural gas into value-added products [48]. Moreover, it does not need any intermediate process as in the dehydration of the ethanol process.

Although there are various methods to perform the partial oxidation of methane, they all consist of four sections, which are: (i) reaction section, (ii) water removal section, (iii) CO_2 capture section, and (iv) ethylene purification section. As shown in Figure 3, firstly, methane and oxygen will be fed into the reactor, and the reaction is exothermic with several side reactions and byproducts. Consequently, rigorous separation processes should be used to purify the product stream from impurities. Therefore, the main challenge in this process is optimizing the reaction to convert more methane into the desired product. The various undesirable reactions that occur in the process have led to more concern about the purification section and how to consume less energy while achieving high product purity. Table 2 shows the main advantages and disadvantages of the OCM process.

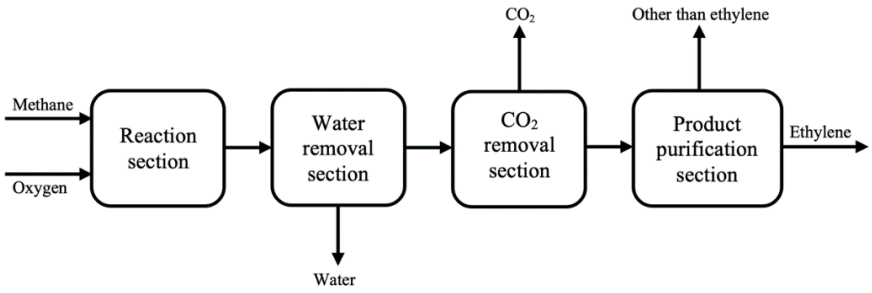

Figure 3. The block flow diagram of the OCM process.

Table 2. The main advantages and disadvantages of the OCM process.

Advantages	Disadvantages
Utilizes an abundant amount of natural gas Low cost of raw material No need for intermediate processes to obtain the feedstock Preserves crude oil from scarcity and depletion Further issues could be resolved with the OCM process, such as utilizing the released methane from biodegradable waste (biogas).	Very stable raw material (low reactivity) Low conversion and selectivity High energy consumption

3. Flowsheet Development of the OCM Process

As mentioned earlier, the OCM process consists of four main sections. In each section, there are different techniques that can be applied, and the choice of the right technique is crucial and has a decisive impact on the profitability of the process. In this part of the

work, each section of the plant will be explained individually before being integrated into a complete process.

3.1. Reaction Section

The feed to the reactor consists of methane and oxygen, and this feed is partially oxidized to produce ethylene, but there will be multiple side products formed, such as C_2H_6, CO_2, CO, H_2, and H_2O. The feed ratio plays an essential role in the reaction conversion and selectivity, where a high CH_4/O_2 ratio leads to high selectivity but low conversion and vice versa [49]. Additionally, the reaction is carried out isothermally with the presence of a catalyst because the hydrocarbon–oxygen mixture tends to be combusted. Many catalysts have been developed and tested for this reaction, but the Li/MgO catalyst has been selected for this work because it is well-studied, and an accurate mathematical model is available [50]. As mentioned earlier, the OCM process confronts many undesired reactions that reduce the yield of the reaction. Table 3 lists the main reactions and side reactions [51].

Table 3. The main and side reactions of the OCM process.

Steps	Reactions	Main/Side
1	$CH_4 + 2O_2 \rightarrow CO_2 + 2H_2O$	Side
2	$2CH_4 + 0.5O_2 \rightarrow C_2H_6 + H_2O$	Main
3	$CH_4 + O_2 \rightarrow CO + H_2O + H_2$	Side
4	$CO + 0.5O_2 \rightarrow CO_2$	Side
5	$C_2H_6 + 0.5O_2 \rightarrow C_2H_4 + H_2O$	Main
6	$C_2H_4 + 2O_2 \rightarrow 2CO + 2H_2O$	Side
7	$C_2H_6 \rightarrow C_2H_4 + H_2$	Side
8	$C_2H_4 + 2H_2O \rightarrow 2CO + 4H_2$	Side
9	$CO + H_2O \rightarrow CO_2 + H_2$	Side
10	$CO_2 + H_2 \rightarrow CO + H_2O$	Side

Indeed, the process of producing ethylene from methane is involved in a gas-phase reaction known as the OCM reaction. However, eight side reactions will take place. Figure S2 shows the reaction scheme. Methane will initially be converted into three parallel reactions, including the formation of ethane by the OCM reaction (step 2), non-selective total oxidation of methane into carbon dioxide (step 1), and partial oxidation of methane to carbon monoxide (step 3). In consecutive steps, ethane proceeds in two parallel reactions, which are heterogeneous catalytic oxidative dehydrogenation of ethane (step 5) and thermal gas-phase dehydrogenation of ethane (step 7). Moreover, carbon monoxide reacts with oxygen to produce carbon dioxide (step 4). It further reacts with steam in a water–gas shift reaction that proceeds in two directions, which are shown in (steps 9 and 10).

3.2. Water Removal Section

Water is one of the byproducts produced in the OCM reactions. It should be adequately removed before the other components are separated because it is the only condensable compound; it can be separated in a cascade of flash drums. If it remains later on in the process, many formidable issues could occur, such as the freezing of water since the separation of non-condensable compounds requires extremely low temperatures.

3.3. Carbon Dioxide Removal Section

The carbon dioxide section is one of the most critical parts of the plant. It has a significant impact on energy consumption, the environment, and product purity. Therefore, the right choice of technique plays a crucial role in the success of the process. There are several techniques that can be applied here, but the most commonly used method is the absorption of CO_2 into the liquid phase by means of a solvent. The choice of solvent is critical in any absorption process, but amine-based solvents are well-known and well-

researched for the absorption of CO_2, and they are well-studied. A mono-ethanolamine (MEA) aqueous solution is the most commonly used solvent for this purpose [52]. MEA usually consists of 30 wt% MEA, the balance being water. The operating pressure in this process is relatively high and requires an efficient compression system [25]. Recent studies have shown that 37% methyl diethanolamine (MDEA) with activated piperazine (PZ) aqueous solutions can lower the absorber pressure [53]. Nevertheless, research studies have proven that the MEA solvent is better than MDEA in terms of absorption efficiency [29]. However, solvent degradation and corrosion are major disadvantages of this absorption method [27].

Additionally, there are other promising processes that could be applied, such as adsorption, which uses solid particles, such as zeolite or activated carbon, that can adsorb CO_2 from the gas phase on the surface of the solid. The adsorption process can reduce the energy consumption significantly by averting using the heating and cooling units for regenerating solvent as in the absorption process [31]. Nevertheless, this process is less effective at removing CO_2 and should be applied in a cascade manner. Moreover, the solid particles need to be replaced after a certain period of time after deactivation. Another promising process is a hybrid system (membrane/absorption process). Although this process offers a reduction in energy consumption costs by about 45%, it results in significant ethylene losses of 15% percent, which is not acceptable [30].

3.4. Ethylene Purification Section

After removing the carbon dioxide, the product stream is purified from the undesired compounds. First, C_2 hydrocarbons (C_2H_4 and C_2H_6) are separated from methane and other light components (CO and H_2). Then, ethylene is separated from ethane, while methane is separated from the other components before being recycled. Figure S3 depicts the product purification section. Normally, three distillation columns are used for this purpose. Nevertheless, adsorption could also be used as it consumes less energy, but there are hidden costs as the product purity will be relatively low, and more stages are required to achieve the same purity, in addition to the large scale that hinders the separation by adsorbers.

3.5. Process Description

The process flow diagram of the OCM process is shown in Figure 4. The numbers from 1-38 indicate the stream numbers. Methane and oxygen are both fed into furnaces to heat up the feed stream before it is fed to the reactor at 810 °C. The effluent from the reactor is cooled to 40 °C before entering the flash drum cascade to separate the non-condensable gasses from the water. The overhead stream from the flash drum, which contains the non-condensable gasses, is fed into the absorber A-101 at a pressure of 12 bar, where almost 96% of the carbon dioxide is removed into the bottom stream by means of MEA–water solvent. The bottom stream from the absorber is heated to 150 °C prior to the stripper, where CO_2 is removed from the solvent and leaves from the top stream while the solvent is purely regenerated to be returned to the absorber after being cooled to 46.5 °C and mixed with a fresh solvent to recover the solvent losses. The overhead stream from the absorber is sent to a caustic wash to remove traces of CO_2. This stream is then compressed to 30 bar and cooled to −25 °C before being fed to the distillation column (T-101), where ethylene and ethane are separated from methane, oxygen, carbon monoxide, and hydrogen. The bottom stream from the previous stage is sent to the distillation column (T-102) to separate ethylene from ethane, with a purity of 99.95%. The overhead stream from (T-101) is sent to the distillation column (T-103) to separate CO and H_2 (syngas) from methane. The bottom stream of (T-103), containing methane, is recycled and mixed with the fresh feed after being expanded to 3 bar.

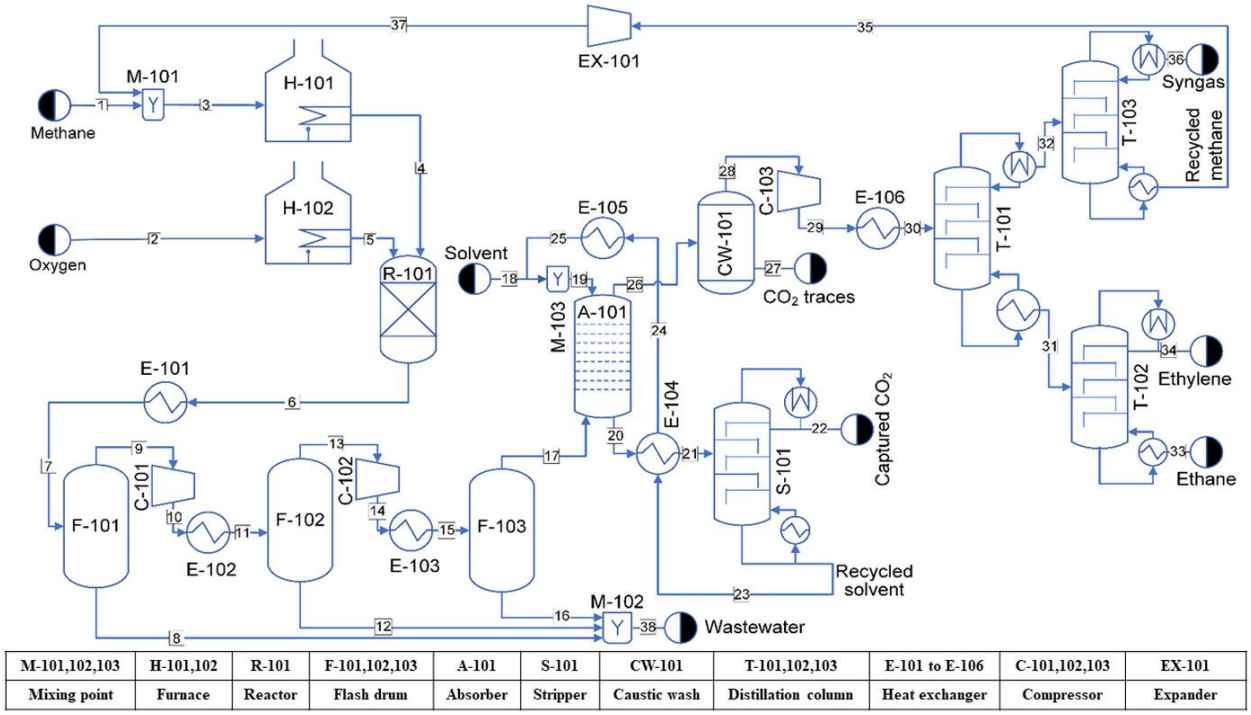

M-101,102,103	H-101,102	R-101	F-101,102,103	A-101	S-101	CW-101	T-101,102,103	E-101 to E-106	C-101,102,103	EX-101
Mixing point	Furnace	Reactor	Flash drum	Absorber	Stripper	Caustic wash	Distillation column	Heat exchanger	Compressor	Expander

Figure 4. Process flow diagram of the OCM plant.

4. Heat Integration

The OCM process requires a significant amount of energy, which currently makes it an undesirable process for many chemical companies. It has a wide temperature range, requiring a high temperature of about 800 °C in the reaction section and about −170 °C in the separation section of the plant. This requires huge external heating and cooling utilities associated with huge costs every year. However, these energies could be seen as an advantage if they are well-integrated. Therefore, pinch analysis was used to construct a network of heat exchangers to minimize the cooling and heating utilities to the threshold values. First, the process streams were identified, and then the temperature interval diagram were plotted to identify the intervals in which exchanging heat between process streams is permissible. An algebraic method was used through the cascade diagrams, in which the minimum heating and cooling utilities were determined. Eventually, a heat exchanger network was constructed to achieve the minimum heating and cooling utilities.

4.1. Stream Identification

The first step in heat integration is to identify the hot and cold streams with their supplied and the target temperatures. In addition, this analysis pertains only to the heat exchangers in the main process stream. Table 4 shows the hot and cold streams that need to be exchanged in the OCM plant.

Table 4. Stream identification of the OCM plant.

Stream	FCp (kJ/K)	$T_{Supplied}$ (°C)	T_{Target} (°C)
2	10.2	25.0	810.0
3	74.1	58.2	810.0
35	75.6	−96.5	73.1
6	87.6	810.0	85.2
10	352.8 *	85.2	40.0
	54.3	120.0	57.8
14	103.4 *	57.8	40.0
	52.6	79.8	48.4
24	254.7	132.2	46.5
29	49.2	129.3	−25.0

* Refers to streams that undergo phase change.

4.2. Determination of the Optimum Value of ΔT_{min}

Heat transfer is restricted by thermal equilibrium. The optimal value of the minimum heat transfer temperature difference ΔT_{min} plays a crucial role in the success of heat integration since a reduction in this value reduces the utility demand at the expense of higher capital costs, and vice versa. Therefore, for the current study on the OCM plant, the Aspen Energy Analyzer v11 was used for the trade-off between the capital and operating costs for different values of ΔT_{min}. Figure S4 shows that for a ΔT_{min} of 25 °C, the total annualized cost reaches the threshold value. Therefore, the pinch analysis in this study was based on ΔT_{min} = 25 °C.

4.3. Temperature–Interval Diagram (TID)

The temperature–interval diagram was drawn, including all the identified streams. The diagram ensures the thermodynamic feasibility of transferring energy between process streams by identifying the exchangeable heat load in each interval, where heat can only be exchanged within the same interval, and the surplus heat is transferred as heat residual to the next interval. The diagram contains two temperature scales for the hot and cold streams. Each stream is represented by an arrow, with the tail representing its supplied temperature and the head representing its target temperature.

Next, the horizontal lines were drawn at the heads and tails of the arrows, where they define the temperature intervals. In addition, each stream was drawn with its corresponding *FCp* either above it or below it. Figure 5 shows the temperature interval diagram of the OCM plant.

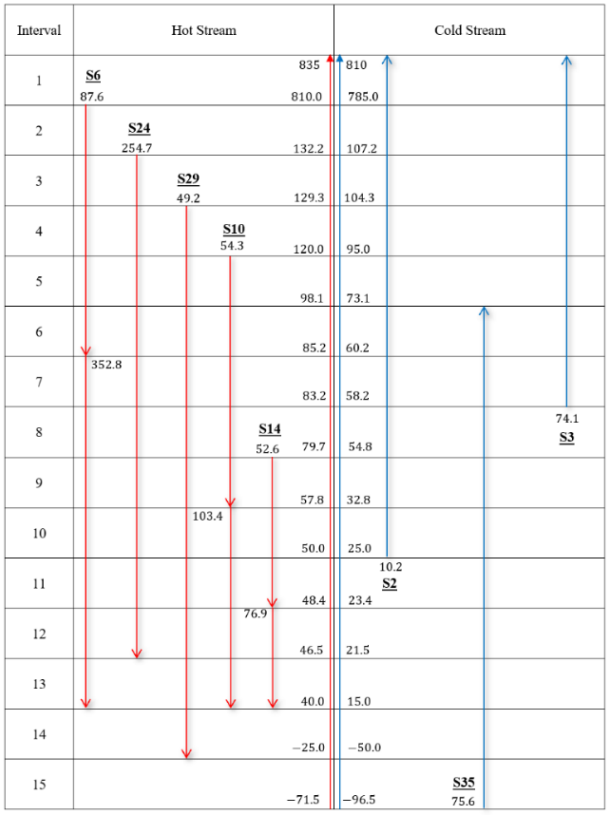

Figure 5. Temperature–interval diagram of the process.

4.4. Exchangeable Heat Load

The exchangeable heat load for each interval determines the amount of energy that is thermodynamically feasible to exchange with another stream; therefore, the intervals represent the boundaries of the heat transfer. Table 5 represents the exchangeable heat load of the hot and cold streams. It shows that the largest amount of energy is in interval 2 because the temperature gradient is relatively higher than the other intervals. Fortunately, a similar amount of energy from the cold streams is in the same interval, allowing the streams to be integrated.

Table 5. The exchangeable heat loads of the process streams for each interval.

Interval	Total Load of the Hot Streams (kW)	Total Load of the Cold Streams (kW)
1	-	2107.5
2	59,375.3	57,138.5
3	992.7	244.5
4	3641.0	784.0
5	9763.0	1846.2
6	5750.8	2062.7
7	1422.0	319.8
8	2488.5	291.7
9	16,722.8	1887.6
10	6339.1	669.2
11	1300.3	121.0
12	1590.3	143.6
13	3785	491.4
14	3198	4914.0
15	-	3515.4

4.5. Cascade and Reversed Cascade Diagrams

The cascade diagram was used to transfer heat between intervals, where the minimum heating and cooling utilities can eventually be determined. The horizontal line represents the hot stream that is thermodynamically feasible to transfer to the cold stream within the same interval. In addition, it is also thermodynamically feasible to transfer the heat in interval z to any cold stream located below it since its temperature is still higher than that of the cold stream. However, transferring heat from interval z to an upper interval is thermodynamically infeasible and is rejected because the temperature of the cold stream will be higher than that of the hot stream.

In the cascade diagram, the minimum heating utility was determined by selecting the most negative value in the train. This value represents the heat deficit after the implementation of heat integration, which must be covered by an external heating utility. On the other hand, the reverse cascade diagram was used to determine the minimum cooling utility, where the remaining value at the end of the train represents the cooling deficit that must be covered by an external cooling utility.

Equation (4) was used to find the remaining energy from each interval [33]. Figure S5 shows the heat balance around a temperature interval.

$$r_z = HH_z^{Total} - HC_z^{Total} + r_{z-1} \quad (4)$$

The cascade diagram was first implemented to determine the minimum heating utility, in which each stream was separated into intervals representing the exchangeable heat load. The left side of Figure 6 shows the cascade diagram (all the values are in kW).

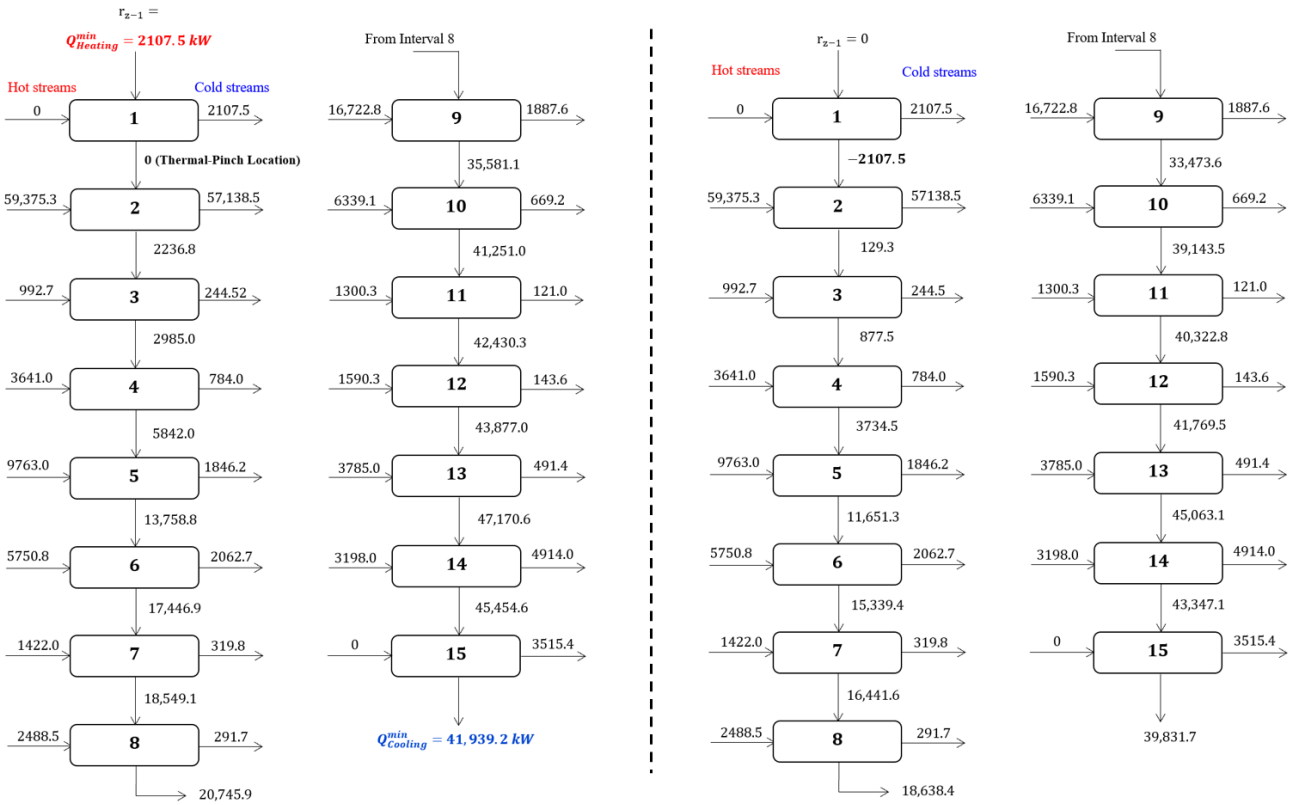

Figure 6. Cascade diagram (**left side**) and revised cascade diagram (**right side**).

The same procedure for the reversed cascade diagram, except for the minimum heating utility, was introduced into the system to find the minimum cooling utility. Figure 6 (right side) represents the reversed cascade diagram (all the values are in kW). As seen in the cascade diagrams, the minimum heating and cooling utilities were 2107.5 kW and

41,939.2 kW, respectively. This highlights that the OCM process confronts cooling deficiency, where a large amount of external cooling utility is required. Nevertheless, the pinch analysis also showed that the implementation of heat integration could add great value to the process by saving a large amount of heating and cooling utilities, which were 76,567.15 kW and 116,397.84 kW before the implementation of heat integration.

4.6. Composite Curves

The pinch analysis was also performed by constructing the composite curve of the hot and cold streams, in which their temperature change was plotted against their enthalpy change. Consequently, the pinch point was identified at the point where the hot and cold stream curves intersect, which is at 800 °C. The minimum heating utility is represented by any cold fluid above the pinch point that can no longer exchange heat with the hot fluid. Likewise, the minimum cooling utility is any hot fluid below the pinch that can no longer exchange heat with the cold fluid. It is worth noting that at ΔT_{min} = 25 °C, the same amount of heating and cooling utilities was obtained. Again, the same results were obtained from this method, where the minimum heating and cooling utilities were 2107.5 kW and 41,939.2 kW, respectively, indicating a more than 95% reduction in the heating utility (from 76,567 kW to 2109 kW) and a more than 60% reduction in cooling utility (from 116,398 kW to 41,939 kW). Consequently, this result shows that the OCM process confronts a cooling deficiency, which requires a huge amount of cooling utility to accomplish the process. Figure 7 represents the thermal pinch diagram of the process.

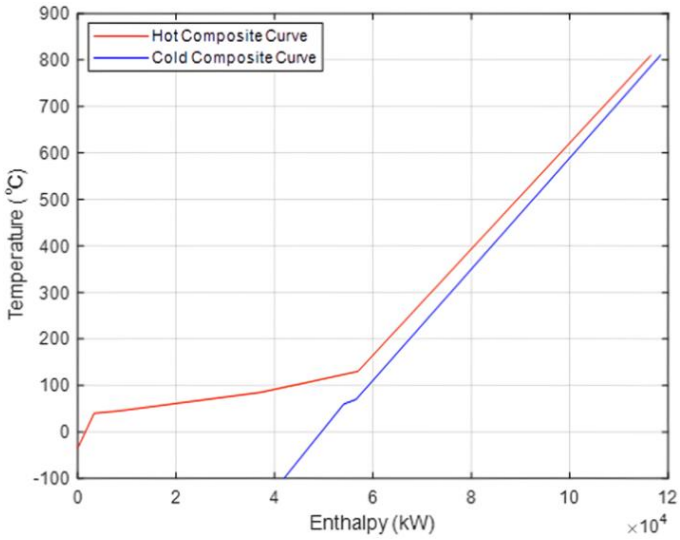

Figure 7. Thermal pinch diagram at ΔT_{min} = 25 °C.

4.7. Heat Exchanger Network (HEN)

In order to achieve this reduction, a heat exchanger network was constructed to find a suitable network that can be implemented in the current OCM plant. Moreover, to implement the heat exchanger network, the intervals must be split into two sections to avoid crossing the pinch point. Figure 8a shows the heat exchanger network above the pinch. There are no hot streams existing above the pinch; therefore, there is no heat integration for these intervals, and only an external heating utility can perform the job. Figure 8b, on the other hand, represents the heat exchanger network below the pinch. It shows that the reactor effluent must be split because the number of cold streams in the interval is greater than of hot streams. In addition, stream 35 can be used to cool streams 29 and 10. This configuration could achieve the minimum heating and cooling utilities obtained through the pinch analysis.

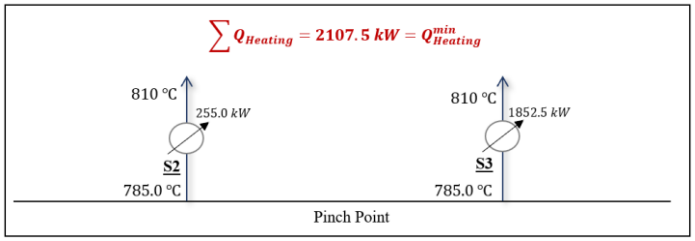

(**a**)

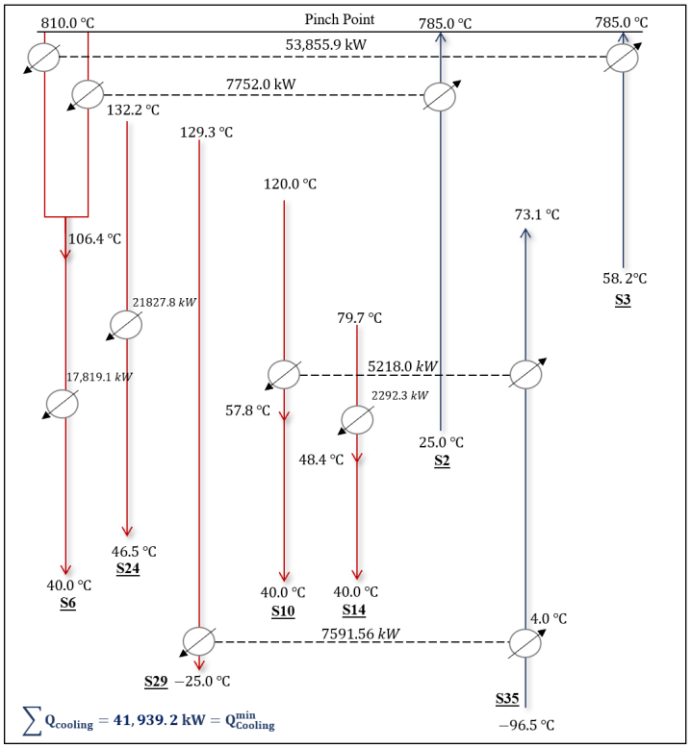

(**b**)

Figure 8. Heat exchanger network (**a**) above the pinch, (**b**) below the pinch.

4.8. The Developed Process Flow Diagram

After conducting the pinch analysis, the bottom stream of T-103 leaving the column at a temperature of −96 °C was used as a coolant for the stream preceding the distillation column T-101 in the heat exchanger E-109. The temperature of stream 37 decreased from 130 °C to −25 °C. Then, the cold stream leaving the heat exchanger E-109 expanded from 30 bar to 4 bar. After being expanded, the stream entered the heat exchanger E-105, which was used in the water removal section to reduce the temperature of the main stream from 120 °C to 40 °C. As a result, the temperature of the cold stream increased to 73 °C before it was mixed with fresh methane. In addition, the reactor effluent with a temperature of 810 °C was split into two streams; each one of them heated each feed stream. Figure 9 shows the process flow diagram after pinch analysis. The numbers from 1-48 indicate the stream numbers.

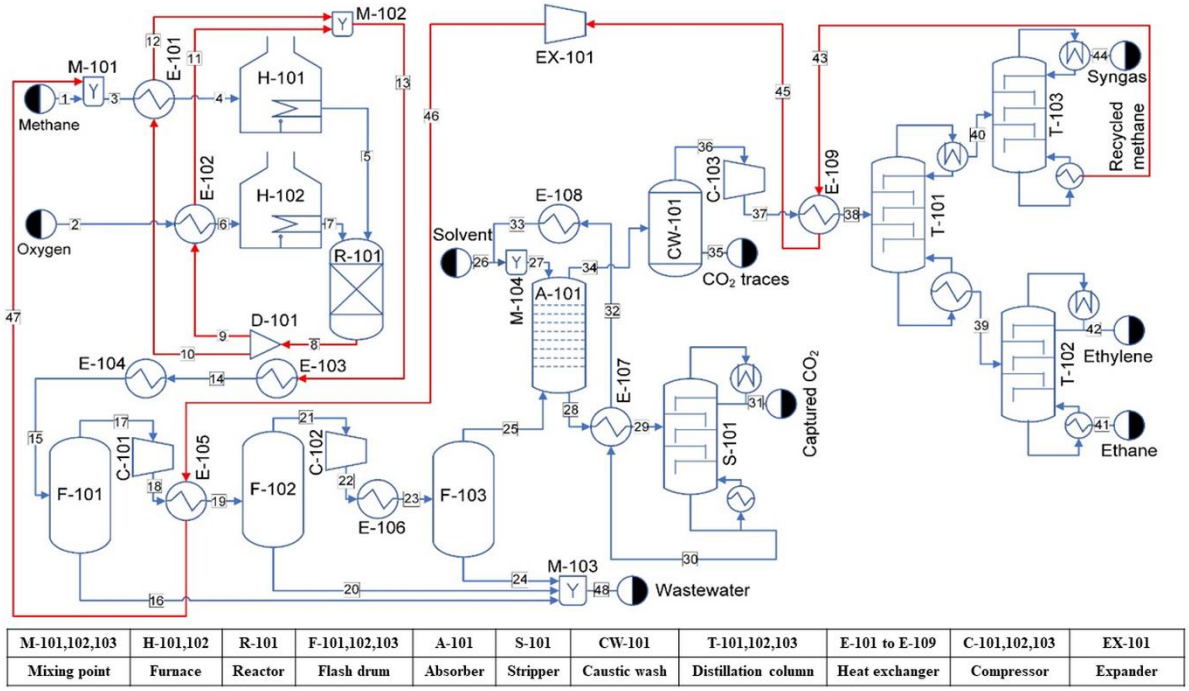

M-101,102,103	H-101,102	R-101	F-101,102,103	A-101	S-101	CW-101	T-101,102,103	E-101 to E-109	C-101,102,103	EX-101
Mixing point	Furnace	Reactor	Flash drum	Absorber	Stripper	Caustic wash	Distillation column	Heat exchanger	Compressor	Expander

Figure 9. Developed process flow diagram of the OCM plant after heat integration.

5. Process Simulation after Heat Integration

A process simulation of the OCM plant with a production rate of 80,000 metric tons of ethylene annually was performed by using Aspen HYSYS v11, as shown in Figure S6. In addition, the process simulation was implemented using the network of heat exchangers obtained from the pinch analysis. The Soave–Redlich–Kwong (SRK) cubic equation of state was selected to describe the non-ideality of the light hydrocarbons in the gas phase. However, for the CO_2-capturing section, an acid–amine gas–chemical solvent fluid package was selected in order to predict all possible reactions between the amine solvent and other components. The kinetics of all reactions and their parameters were taken from [50], achieving a conversion and a selectivity of 31% and 58%, respectively. Figure S7 depicts the molar compositions of the inlet and outlet streams from the reactor, where the left axis refers to the inlet stream and the right axis refers to the outlet stream. The kinetics equations and parameters are provided as supporting information. Although new catalysts may reach higher values for conversion and selectivity, as can be seen in Table 3, there is no validated mathematical model available that could be used in a simulation package. On the other hand, after the water removal stage, the simulation used the acid–amine gas–chemical solvent fluid package for the CO_2-capturing system. The solvent was able to capture 98% of the CO_2 into stream 22. After that, the overhead stream from the absorber A-101 was sent to a caustic wash to remove the traces of CO_2. However, in this part of the simulation, a component separator was used instead because the caustic wash is not available in HYSYS. After that, the simulator was turned into SRK fluid package for the last three distillation columns that were used for the purification of the product and recycling of the unreacted materials. The result of the overhead stream from the distillation column T-102 shows that the ethylene reached a polymer-grade purity of 99.95% [54]. Table S1 shows the results of the main streams obtained from the simulation. The executable Aspen HYSYS file for the process after heat integration is provided as Supplementary Materials.

Converting the High Exothermic Reaction Heat into Power Production

The OCM reactor comprises highly exothermic reactions that release 96.5 MW of heat. In order to operate the reactor isothermally, this large amount of heat must be removed through a cooling system, resulting in huge utility cost. However, an analog to the power

production cycle could be implemented in this process coupled with the cooling jacket side to produce electricity. A similar idea has been suggested for other processes by Greef et al. [55] and Li et al. [56] to recover exothermic reaction heat using turbine expanders. In fact, the power production cycle usually consists of four main components: (1) pump, (2) boiler, (3) turbine, and (4) condenser. A schematic representation of this power plant is depicted in Figure 10.

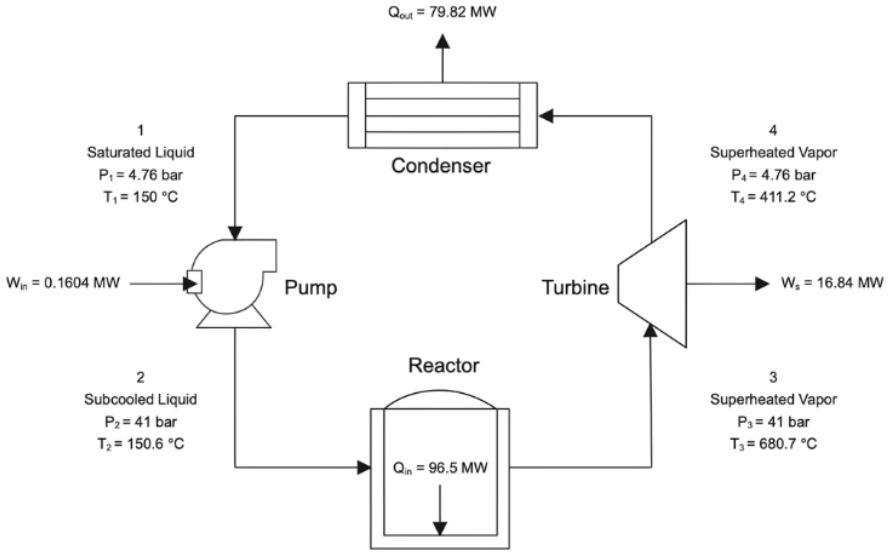

Figure 10. Power production cycle coupled with the OCM reactor jacket.

The source of the heat in the boiler is the main concern in such a cycle. However, since the OCM reactor releases a large amount of heat due to the highly exothermic reactions, the reactor can play the role of a boiler. The 96.5 MW of heat added to the cooling system will deliver a net shaft work of 16.68 MW at an efficiency of 75%. The generated electricity can then be utilized to deliver the process compressors, which require total power of 10.1 MW. The main outcome of the cycle is a complete elimination of all the compressors power, resulting in large savings in the utility cost. The Aspen HYSYS executable file for this power plant is provided as Supplementary Materials.

6. Conclusions

Due to the expedited production of natural gas, many researchers are working to find new routes for the conversion of methane into highly valuable petrochemical products. The OCM process is considered one of the most intriguing routes of the conversion of methane into ethylene, a key building block product of the petrochemical industry. Indeed, ethylene consumption is continuously growing to meet the global demand for its versatile derivatives, such as polyethylene, polystyrene, and ethylene glycol. Nevertheless, the OCM process suffers from many drawbacks, such as requiring a very high temperature for the reaction, therefore competing with the combustion reactions. The process also requires very low temperatures for the separation of the light hydrocarbons, increasing the necessity for heat integration. Heat integration based on pinch analysis was implemented for the main process streams, indicating that the heating and cooling utilities can be reduced from 76,567 kW and 116,398 kW to 2107.5 kW and 41,939 kW, respectively, at an optimum ΔT_{min} of 25 °C obtained by compromising between the capital and operating costs using Aspen Energy Analyzer v11. The results emphasize that the OCM process can compete with other exiting processes. In addition, the process was simulated using Aspen HYSYS v11, verifying the obtained results.

Finally, the OCM reactor involves highly exothermic reactions that release 96.5 MW of heat. Consequently, a further enhancement of the process has been proposed in this work by recovering the high exothermic reaction heat through a steam power plant coupled with

the reactor jacket. It was found that the generated electricity can be used to cover the huge energy demand for the process compressors.

Supplementary Materials: The following supporting information can be downloaded at: https://www.mdpi.com/article/10.3390/pr10061085/s1. Figure S1: Ethylene consumption by application; Figure S2: Reaction scheme; Figure S3: Ethylene purification section breakdown; Figure S4: Temperature–interval diagram of the process; Figure S5: Heat balance around a temperature interval; Figure S6: Process simulation of the OCM plant; Figure S7: Molar composition profile for the inlet and outlet streams of the reactor; Table S1: Key streams results obtained from the simulation.

Author Contributions: Conceptualization, M.B. and M.K.H.-K.; methodology, R.A., A.A., I.W. and M.K.H.-K.; software, R.A. and A.A.; validation, R.A., A.A. and M.K.H.-K.; formal analysis, M.B. and I.W.; investigation, R.A., A.A. and M.K.H.-K.; resources, R.A., A.A., M.B. and I.W.; data curation, R.A., A.A. and M.K.H.-K.; writing—R.A., A.A., I.W. and M.K.H.-K.; writing—review and editing, R.A., A.A., I.W. and M.K.H.-K.; supervision, M.B. and M.K.H.-K.; project administration, M.B. and M.K.H.-K.; funding acquisition, M.K.H.-K. All authors have read and agreed to the published version of the manuscript.

Funding: The authors would like to express their appreciation to the Researchers Supporting Project (RSP-2021/361), King Saud University, Riyadh, Saudi Arabia, for the financial support.

Institutional Review Board Statement: Not applicable.

Informed Consent Statement: Not applicable.

Data Availability Statement: Not applicable.

Conflicts of Interest: The authors declare no conflict of interest.

References

1. Karakaya, C.; Zhu, H.; Zohour, B.; Senkan, S.; Kee, R.J. Detailed reaction mechanisms for the oxidative coupling of methane over La2O3/CeO2 nanofiber fabric catalysts. *Chem. Cat. Chem.* **2017**, *9*, 4538–4551.
2. Liu, J.; Yue, J.; Lv, M.; Wang, F.; Cui, Y.; Zhang, Z.; Xu, G. From fundamentals to chemical engineering on oxidative coupling of methane for ethylene production: A review. *Carbon Resour. Convers.* **2022**, *5*, 1–14. [CrossRef]
3. Galli, F.; Lai, J.-J.; De Tommaso, J.; Pauletto, G.; Patience, G.S. Gas to Liquids Techno-Economics of Associated Natural Gas, Bio Gas, and Landfill Gas. *Processes* **2021**, *9*, 1568. [CrossRef]
4. Ridha, T.; Li, Y.; Gençer, E.; Siirola, J.J.; Miller, J.T.; Ribeiro, F.H.; Agrawal, R. Valorization of shale gas condensate to liquid hydrocarbons through catalytic dehydrogenation and oligomerization. *Processes* **2018**, *6*, 139. [CrossRef]
5. Ethylene Market Share, Size, Trends, Industry Analysis Report by Feedstock (Naphtha, Ethane, Propane, Butane); By Application (Polyethylene, Ethylene Oxide, Ethyl Benzene, Ethylene Dichloride); By End-Use; By Region, Segment Forecast, 2021–2029. Available online: https://www.polarismarketresearch.com/industry-analysis/ethylene-market (accessed on 5 April 2022).
6. Cruellas, A.; Bakker, J.; van Sint Annaland, M.; Medrano, J.; Gallucci, F. Techno-economic analysis of oxidative coupling of methane: Current state of the art and future perspectives. *Energy Convers. Manag.* **2019**, *198*, 111789. [CrossRef]
7. Galadima, A.; Muraza, O. Revisiting the oxidative coupling of methane to ethylene in the golden period of shale gas: A review. *J. Ind. Eng. Chem.* **2016**, *37*, 1–13. [CrossRef]
8. Karakaya, C.; Kee, R.J. Progress in the direct catalytic conversion of methane to fuels and chemicals. *Prog. Energy Combust. Sci.* **2016**, *55*, 60–97. [CrossRef]
9. Spallina, V.; Velarde, I.C.; Jimenez, J.A.M.; Godini, H.R.; Gallucci, F.; Annaland, M.V.S. Techno-economic assessment of different routes for olefins production through the oxidative coupling of methane (OCM): Advances in benchmark technologies. *Energy Convers. Manag.* **2017**, *154*, 244–261. [CrossRef]
10. Cheng, Z.; Baser, D.S.; Nadgouda, S.G.; Qin, L.; Fan, J.A.; Fan, L.-S. C2 selectivity enhancement in chemical looping oxidative coupling of methane over a Mg–Mn composite oxygen carrier by Li-doping-induced oxygen vacancies. *ACS Energy Lett.* **2018**, *3*, 1730–1736. [CrossRef]
11. Gao, Y.; Neal, L.; Ding, D.; Wu, W.; Baroi, C.; Gaffney, A.M.; Li, F. Recent advances in intensified ethylene production—A review. *ACS Catal.* **2019**, *9*, 8592–8621. [CrossRef]
12. Natural Gas and the Environment—U.S. Energy Information Administration (EIA). Available online: https://www.eia.gov/energyexplained/natural-gas/natural-gas-and-the-environment.php (accessed on 12 March 2022).
13. Murthy, P.R.; Liu, Y.; Wu, G.; Diao, Y.; Shi, C. Oxidative Coupling of Methane: Perspective for High-Value C2 Chemicals. *Crystals* **2021**, *11*, 1011. [CrossRef]
14. Baser, D.S.; Cheng, Z.; Fan, J.A.; Fan, L.-S. Codoping Mg-Mn Based Oxygen Carrier with Lithium and Tungsten for Enhanced C2 Yield in a Chemical Looping Oxidative Coupling of Methane System. *ACS Sustain. Chem. Eng.* **2021**, *9*, 2651–2660. [CrossRef]

15. Fleischer, V.; Steuer, R.; Parishan, S.; Schomäcker, R. Investigation of the surface reaction network of the oxidative coupling of methane over Na2WO4/Mn/SiO2 catalyst by temperature programmed and dynamic experiments. *J. Catal.* **2016**, *341*, 91–103. [CrossRef]
16. Gu, B.; Ordomsky, V.V.; Bahri, M.; Ersen, O.; Chernavskii, P.A.; Filimonov, D.; Khodakov, A.Y. Effects of the promotion with bismuth and lead on direct synthesis of light olefins from syngas over carbon nanotube supported iron catalysts. *Appl. Catal. B Environ.* **2018**, *234*, 153–166. [CrossRef]
17. Meng, F.; Li, X.; Zhang, P.; Yang, L.; Yang, G.; Ma, P.; Li, Z. Highly active ternary oxide ZrCeZnOx combined with SAPO-34 zeolite for direct conversion of syngas into light olefins. *Catal. Today* **2021**, *368*, 118–125. [CrossRef]
18. Salkuyeh, Y.K.; Adams II, T.A. A novel polygeneration process to co-produce ethylene and electricity from shale gas with zero CO2 emissions via methane oxidative coupling. *Energy Convers. Manag.* **2015**, *92*, 406–420. [CrossRef]
19. Toraman, H.E.; Alexopoulos, K.; Oh, S.C.; Cheng, S.; Liu, D.; Vlachos, D.G. Ethylene production by direct conversion of methane over isolated single active centers. *Chem. Eng. J.* **2021**, *420*, 130493. [CrossRef]
20. Keller, G.; Bhasin, M. Synthesis of ethylene via oxidative coupling of methane: I. Determination of active catalysts. *J. Catal.* **1982**, *73*, 9–19. [CrossRef]
21. Ito, T.; Lunsford, J.H. Synthesis of ethylene and ethane by partial oxidation of methane over lithium-doped magnesium oxide. *Nature* **1985**, *314*, 721–722. [CrossRef]
22. Hinsen, W.; Bytyn, W.; Baerns, M. Oxidative Dehydrogenation and Coupling of Methane. In Proceedings of the 8th International Congress on Catalysis, Berlin, Germany, 2–6 July 1984; p. 581.
23. Driscoll, D.J.; Martir, W.; Wang, J.X.; Lunsford, J.H. Formation of gas-phase methyl radicals over magnesium oxide. *J. Am. Chem. Soc.* **1985**, *107*, 58–63. [CrossRef]
24. Da Ros, S.; Barbalho Fontoura, T.; Schwaab, M.; Castro de Jesus, N.J.; Pinto, J.C. Oxidative Coupling of Methane for Ethylene Production: Reviewing Kinetic Modelling Approaches, Thermodynamics and Catalysts. *Processes* **2021**, *9*, 2196. [CrossRef]
25. Godini, H.R.; Azadi, M.; Khadivi, M.; Gharibi, A.; Jazayeri, S.M.; Salerno, D.; Penteado, A.; Mokhtarani, B.; Orjuela, A.; Karsten, T. Conceptual Process Design and Economic Analysis of Oxidative Coupling of Methane. In *Computer Aided Chemical Engineering*; Elsevier: Amsterdam, The Netherlands, 2018; Volume 44, pp. 361–366.
26. Elkins, T.W.; Neumann, B.R.; Bäumer, M.; Hagelin-Weaver, H.E. Effects of Li Doping on MgO-Supported Sm2O3 and TbO x Catalysts in the Oxidative Coupling of Methane. *ACS Catal.* **2014**, *4*, 1972–1990. [CrossRef]
27. Lee, I.Y.; Kwak, N.S.; Lee, J.H.; Jang, K.R.; Shim, J.-G. Degradation and corrosivity of MEA with oxidation inhibitors in a carbon dioxide capture process. *J. Chem. Eng. Jpn.* **2012**, *45*, 343–347. [CrossRef]
28. Penteado, A.T.; Kim, M.; Godini, H.R.; Esche, E.; Repke, J.-U. Techno-economic evaluation of a biogas-based oxidative coupling of methane process for ethylene production. *Front. Chem. Sci. Eng.* **2018**, *12*, 598–618. [CrossRef]
29. Hasan, S.; Abbas, A.J.; Nasr, G.G. Improving the carbon capture efficiency for gas power plants through amine-based absorbents. *Sustainability* **2020**, *13*, 72. [CrossRef]
30. Radaelli, G.; Chachra, G.; Jonnavittula, D. *Low-Energy, Low-Cost Production of Ethylene by Low-Temperature Oxidative Coupling of Methane*; Siluria Technologies, Inc.: San Francisco, CA, USA, 2017.
31. Krishnaiah, D.; Bono, A.; Anisuzzaman, S.; Joseph, C.; Khee, T.B. Carbon dioxide removal by adsorption. *J. Appl. Sci.* **2014**, *14*, 3142–3148. [CrossRef]
32. Geankoplis, C.J. *Transport Processes and Unit Operations*; Allyn and Bacon: Boston, MA, USA, 1978.
33. El-Halwagi, M.M. *Sustainable Design Through Process Integration: Fundamentals and Applications to Industrial Pollution Prevention, Resource Conservation, and Profitability Enhancement*; Elsevier Science: Amsterdam, The Netherlands, 2017.
34. Arndt, S.; Simon, U.; Heitz, S.; Berthold, A.; Beck, B.; Görke, O.; Epping, J.-D.; Otremba, T.; Aksu, Y.; Irran, E. Li-doped MgO from different preparative routes for the oxidative coupling of methane. *Top. Catal.* **2011**, *54*, 1266–1285. [CrossRef]
35. Gunardson, H.H. *Industrial Gases in Petrochemical Processing: Chemical Industries*; CRC Press: Boca Raton, FL, USA, 1997.
36. Bao, X.; Xu, Y. Steam reforming of hydrocarbons. A historical perspective. In Proceedings of the Natural Gas Conversion VII: The 7th Natural Gas Conversion Symposium, Dalian, China, 6–10 June 2004.
37. Ortiz-Bravo, C.A.; Chagas, C.A.; Toniolo, F.S. Oxidative coupling of methane (OCM): An overview of the challenges and opportunities for developing new technologies. *J. Nat. Gas Sci. Eng.* **2021**, *96*, 104254. [CrossRef]
38. Tiyatha, W.; Chukeaw, T.; Sringam, S.; Witoon, T.; Chareonpanich, M.; Rupprechter, G.; Seubsai, A. Oxidative coupling of methane—comparisons of MnTiO3–Na2WO4 and MnOx–TiO2–Na2WO4 catalysts on different silica supports. *Sci. Rep.* **2022**, *12*, 2595. [CrossRef]
39. Vandewalle, L.A.; Van de Vijver, R.; Van Geem, K.M.; Marin, G.B. The role of mass and heat transfer in the design of novel reactors for oxidative coupling of methane. *Chem. Eng. Sci.* **2019**, *198*, 268–289. [CrossRef]
40. Zhang, M.; Yu, Y. Dehydration of ethanol to ethylene. *Ind. Eng. Chem. Res.* **2013**, *52*, 9505–9514. [CrossRef]
41. Okagami, A.; Matsuoka, S. Process for Manufacturing Olefins by Catalytic Partial Oxidation of Hydrocarbons. Google Patents US 3541179, 17 November 1970.
42. Application Solution Guide Ethylene. Available online: https://empoweringpumps.com/white-papers/flowserve-application-solutions-guide-for-ethylene/ (accessed on 5 April 2022).
43. Cameron, G.; Le, L.; Levine, J.; Nagulapalli, N. Process design for the production of ethylene from ethanol. *Sr. Des. Rep.* **2012**, *39*.
44. Morschbacker, A. Bio-ethanol based ethylene. *J. Macromol. Sci. ®Part C Polym. Rev.* **2009**, *49*, 79–84. [CrossRef]

45. Chen, Y. *Simulation and Synthesis of Heat Exchange Networks for Producing Ethylene from Ethanol*; Tianjin University: Tianjin, China, 2007.
46. Bashir, A.; Malik, L.A.; Ahad, S.; Manzoor, T.; Bhat, M.A.; Dar, G.; Pandith, A.H. Removal of heavy metal ions from aqueous system by ion-exchange and biosorption methods. *Environ. Chem. Lett.* **2019**, *17*, 729–754. [CrossRef]
47. "Soft" Oxidative Coupling of Methane to Ethylene: Mechanistic Insights from Combined Experiment and Theory. Available online: https://www.pnas.org/doi/10.1073/pnas.2012666118 (accessed on 22 January 2022).
48. Kiani, D.; Sourav, S.; Baltrusaitis, J.; Wachs, I.E. Oxidative coupling of methane (OCM) by SiO2-supported tungsten oxide catalysts promoted with Mn and Na. *ACS Catal.* **2019**, *9*, 5912–5928. [CrossRef]
49. Rattananon, N.; Assabumrungrat, S.; Arpornwichanop, A.; Putivisutisak, S.; Wiyaratn, W. Analysis of an Oxidative Coupling of Methane (OCM) Reactor: Multi Point Feeding Policy. In Proceedings of the TIChE International Conference, Hatyai, Thailand, 10–11 November 2011.
50. Vatani, A.; Jabbari, E.; Askarieh, M.; Torangi, M.A. Kinetic modeling of oxidative coupling of methane over Li/MgO catalyst by genetic algorithm. *J. Nat. Gas Sci. Eng.* **2014**, *20*, 347–356. [CrossRef]
51. Stansch, Z.; Mleczko, L.; Baerns, M. Comprehensive kinetics of oxidative coupling of methane over the La2O3/CaO catalyst. *Ind. Eng. Chem. Res.* **1997**, *36*, 2568–2579. [CrossRef]
52. Reynolds, A.; Verheyen, T.; Meuleman, E. Degradation of amine-based solvents. In *Absorption-Based Post-combustion Capture of Carbon Dioxide*; Elsevier: Amsterdam, The Netherlands, 2016; pp. 399–423.
53. Esche, E.; Arellano-Garcia, H.; Wozny, G.; Biegler, L. Optimal Operation of a Membrane Reactor Network. In *Computer Aided Chemical Engineering*; Elsevier: Amsterdam, The Netherlands, 2012; Volume 31, pp. 1321–1325.
54. Ethylene. Available online: https://www.dow.com/en-us/pdp.ethylene.31681z.html#overview (accessed on 5 April 2022).
55. Greeff, I.; Visser, J.; Ptasinski, K.; Janssen, F. Using turbine expanders to recover exothermic reaction heat—Flow sheet development for typical chemical processes. *Energy* **2004**, *29*, 2045–2060. [CrossRef]
56. Li, G.; Zhong, G.; Wu, Q. Study on integrating a gas turbine in steam methane reforming process. *Appl. Therm. Eng.* **2016**, *99*, 919–927. [CrossRef]